THE SQUID GIANT AXON

MATHEMATICAL MODELS

ROSALIE C. HOYT
From the Physics Department, Bryn Mawr College, Bryn Mawr, Pennsylvania

ABSTRACT The voltage clamp results of Hodgkin and Huxley have been reanalyzed in terms of alternative mathematical models. The model used for the potassium conductance changes is similar to that of the HH model except that an empirical functional relationship replaces the fourth power Law used by HH and the twenty-fifth power law used by Cole and Moore. The model used for the sodium conductance changes involves the explicit use of one variable only rather than the two variables m and h of HH. The rise and fall of the sodium conductance during a depolarizing voltage clamp is obtained by specifying that this one variable satisfies a second order differential equation which results from the coupling of two first order equations. Not only can the adjustable parameters of these models be made to give good fit to the clamp conductance data but the models can also then be used to compute action potential curves. Theoretical interpretations can also be given to these mathematical models.

INTRODUCTION

With the exception of one modification recently found necessary by Cole and Moore (1) the original equations of Hodgkin and Huxley (2) still seem after 10 years to represent exceedingly well the behavior of the normal squid axon. Yet, as pointed out by Hodgkin and Huxley these equations probably do not represent the only mathematical model that can be fitted to the experimental data. If this is true, then the type of chemicophysical model suggested by the Hodgkin and Huxley equations may not be the only type that can be suggested for the membrane mechanisms responsible for the active response. Other mathematical models should suggest other types of physical or chemical models. If more than the one physical model were available, further experiments might aid in possibly distinguishing between the models and thus help to arrive at a clearer picture of the actual mechanisms involved in the membrane reactions.

Over the past few years several new mathematical models have been investigated by the author to see if they can be made to fit the original Hodgkin and Huxley experimental data. The results obtained to date on one such pair of models (one for the behavior of the potassium conductance and one for the behavior of the sodium conductance) are presented below, together with the resulting (normal) membrane

action potentials obtained with this pair of mathematical models. The model used for the potassium conductance changes is very similar to that of Hodgkin and Huxley (2), except that the assumption of a simple power law dependence of g_K on the variable n is not made. Instead of a power law, a functional dependence has been determined to give the best fit to the experimental clamp data. The model used for the sodium conductance assumes that the dependence is on only one variable instead of the two variables m and h of Hodgkin and Huxley. The rise and fall of g_{Na} is obtained by assuming that this one variable satisfies a second order differential equation rather than a first order one. Again as in the potassium case, the functional dependence of g_{Na} on this single variable is not assumed to be that of a simple power law, rather it has been chosen to give the best fit of the computed clamp curves to the Hodgkin and Huxley experimental data.

In the years since their first development, the Hodgkin and Huxley equations (2) have been modified to fit a number of situations other than those for which they were originally devised. For example, by simple parameter changes it has been found possible to fit the Hodgkin and Huxley equations to the results of Tasaki and others (3, 4) on TEA-(tetraethylammonium chloride) treated fibers (FitzHugh, 5). By similar parameter adjustments Noble (6) has been able to account for the action and pacemaker potentials of Purkinje fibers. Any useful alternative to the Hodgkin and Huxley model must therefore also be able to account for more than the electrical behavior of squid fibers under normal environmental conditions. The present paper reports only on the results of fitting the new models to the original clamp data and the computation of normal squid action potentials. Attempts to modify the new models to account for the larger body of experimental information is planned for the near future.

METHOD

Although Cole and Moore (7) have recently pointed out a number of experimental artifacts that undoubtedly are often present in the data obtained by the voltage clamp method, the experimental results of Hodgkin, Huxley, and Katz (8) and of Hodgkin and Huxley (2, 9–11)[1] can still be considered to represent quite well the experimental behavior of the squid axon under more or less normal ionic conditions. These results have therefore been taken as the basis of the present analysis. Although questioned by Tasaki and Hagiwara (3), separation of the clamp currents into the two major fractions, a sodium and a potassium current, is accepted. The basic equivalent circuit, shown in Fig. 1, is thus the same as that of fig. 1 of HH (2),[2] with the potassium and sodium conductances, g_K and g_{Na}, being functions of the membrane voltage and time.

Most of the present work has been based on the data presented in figs. 3 and 6 of HH (2) for their axon 17. These clamp conductance data for axon 17 have been reanalyzed

[1] Hereafter the Hodgkin and Huxley papers will be referred to as HH (2), HH (9), etc.

[2] As an aid to clarity, references to figures and equations in this paper will be capitalized as Fig. 1, Eq. (1), etc., while reference to figures in the HH and other papers will be given as fig. 1, eq. (1), etc.

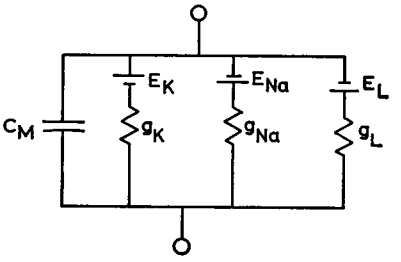

FIGURE 1 Membrane equivalent circuit.

in terms of new mathematical models, leading to new equations and empirical curves to replace the equations given at the beginning of part III of HH (2). The new equations and curves have in turn been used to compute membrane action potentials to compare with HH (2) fig. 12, or Hodgkin, Huxley, and Katz (8) fig. 9.

The numerical integrations necessary for computation of these membrane action potentials were originally done by desk calculator methods, but have recently been checked on an IBM 1620 digital computer. No attempt has as yet been made to compute propagated action potentials.

As in the HH (2) treatment, the membrane voltage, V, will be referred to the resting potential as an origin; thus $V = E - E_r$ where E is the potential difference across the membrane and E_r is its resting value. The original sign convention of HH is used throughout the present report, except that depolarizing voltages are considered positive.

THE POTASSIUM CONDUCTANCE

Typically, the potassium conductance, g_K, under a depolarizing clamp rises monotonically along a sigmoid curve, approaching a final equilibrium value that increases with the magnitude of the clamp. Hodgkin and Huxley (2) were able to obtain a close approximation to the characteristic shape of the rise of g_K with time, with its very marked initial delay, by assuming that g_K is *directly* proportional to the fourth power of a variable n which increases exponentially from its initial value n_0 to its final equilibrium value n_∞. Cole and Moore (1) have shown that a considerably higher power than the fourth may be necessary.

In the present analysis it is assumed that g_K depends on a variable v_k, analogous to the HH variable n, but relabeled to distinguish the two models. For convenience v_k is taken to be zero in the resting state at the normal equilibrium voltage ($V = 0$). No loss of generality is obtained in making this choice. The time dependence of v_k under voltage clamp conditions is, as for the variable n in the HH case, taken to be given by a first order differential equation,

$$\frac{dv_k}{dt} = a_k(v_{k\infty} - v_k), \tag{1}$$

with solutions given by

$$v_k = v_{k\infty}(1 - e^{-a_k t}), \tag{2}$$

where the parameters $v_{k\infty}$ and a_k are dependent on the membrane voltage only.

The functional relationship, $g_K = g_K(v_k)$, and the voltage dependence of $v_{k\infty}$ and a_k, are to be chosen so that as v_k increases exponentially with time the conductance, $g_K = g_K(v_k) = g_K(t)$, increases with time along a curve that is, for each clamp voltage, in agreement with the corresponding HH clamp curve.

The procedure used to deduce the $g_K(v_k)$ curve is outlined in Appendix I, and the resulting empirically determined curve is shown in Fig. 2. It should be noted

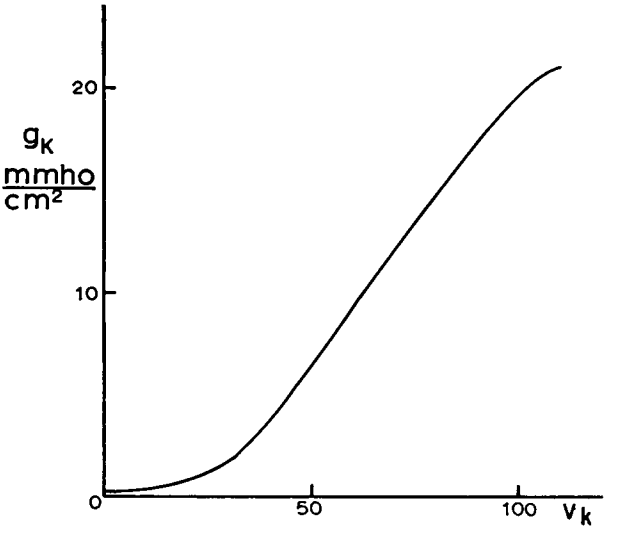

FIGURE 2 Dependence of the potassium conductance on the variable v_k.

that the curve of Fig. 2 can not be fitted by a simple power law of the form of $g_K = \bar{g}_K(v_k + C)^n$. For small values of g_K the behavior is close to that of a power law, but for larger values of g_K the slope does not continue to increase as it must for a power law.

For each different clamp voltage, as v_k increases exponentially to its final value $v_\infty(V)$, the conductance correspondingly climbs up the curve of Fig. 2 to a final equilibrium value $g_{K\infty}$ given by $g_{K\infty} = g_K(v_{k\infty})$. The time course of the rise of g_K along this curve to its final value is determined by the value of the rate constant $a_k(V)$. The dependence of $v_{k\infty}$ and a_k on the clamping voltage V, again chosen to give the best fit to the experimental curves, are shown in Fig. 3.

The curve of Fig. 2 and the points shown in Fig. 3 were chosen to give fits to the experimental clamps used by HH (*i.e.* 6, 10, 19, 26, 32, 38, 51, 63, 76, 88, 100, and 109 mv). The resulting computed clamp curves are shown by the solid lines in Fig. 4. Where the curves computed by HH differ from those computed here, the former are shown by dashed lines. It can be seen that the solid curves are in general better able to reproduce the slow initial rise than the dashed curves.

In this model, then, the curve of Fig. 2 replaces the power law equation of HH,

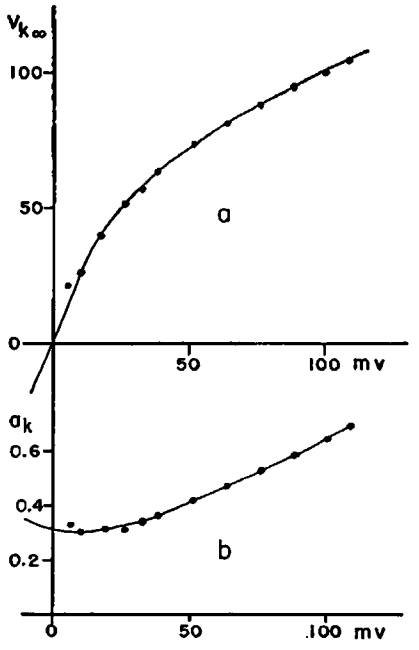

FIGURE 3 Dependence of the potassium parameters $v_{k\infty}$ and a_k on the clamping voltage. The points represent the values used in computing the conductance curves of Fig. 4. The curves fitted to these points were used in computing the membrane action potential curves of Figs. 14 and 15. The ordinate scale for a_k is in $(\text{msec.})^{-1}$.

while the smooth curves drawn through the $v_{k\infty}$ and a_k points in Fig. 3 replaces the HH equations for the voltage dependence of α_n and β_n (eqs. 12 and 13 of HH (2)). Using the curves of Fig. 3 one can for any arbitrary clamp voltage, V, read off the appropriate values of a_k and $v_{k\infty}$. These then allow one to compute, from Eq. 2, the values of v_k as a function of time for this clamp voltage, V. Using these values of $v_k(t)$ one can then determine the corresponding $g_K(t)$ from Fig. 2. (See Fig. 18 in Appendix I).

The g_K versus v_k curve of Fig. 2 was chosen to give the best fit to the HH clamp data on axon 17 only, and may therefore not be representative of an average squid axon in good condition. Examination of table 3 of HH (2) shows that their parameter $\bar{g}_K$ varied considerably from fiber to fiber. This variability can be obtained in the present model by simple scale changes in the ordinate of Fig. 2 without any changes in shape. In particular a comparison of the value given for $\bar{g}_K$ of axon 17 in table 1 of HH (2) with the value chosen by them as representative (table 3 of the same paper) shows that for a more representative fiber all ordinates on the left in Fig. 2 should probably be multiplied by a factor of about 1.6.

After account is taken of such scale changes, there remains the question of the generality of the specific shape of the g_K versus v_k curve. One simple test of generality has been made by plotting, for $\Delta V = 109$, the calculated values of $\log g_K(t)$ against $\log (t + t_0)/\tau$ where t_0 and τ are adjustable parameters. Cole and Moore (1) have shown that for clamps to the sodium potential, starting from close to the rest-

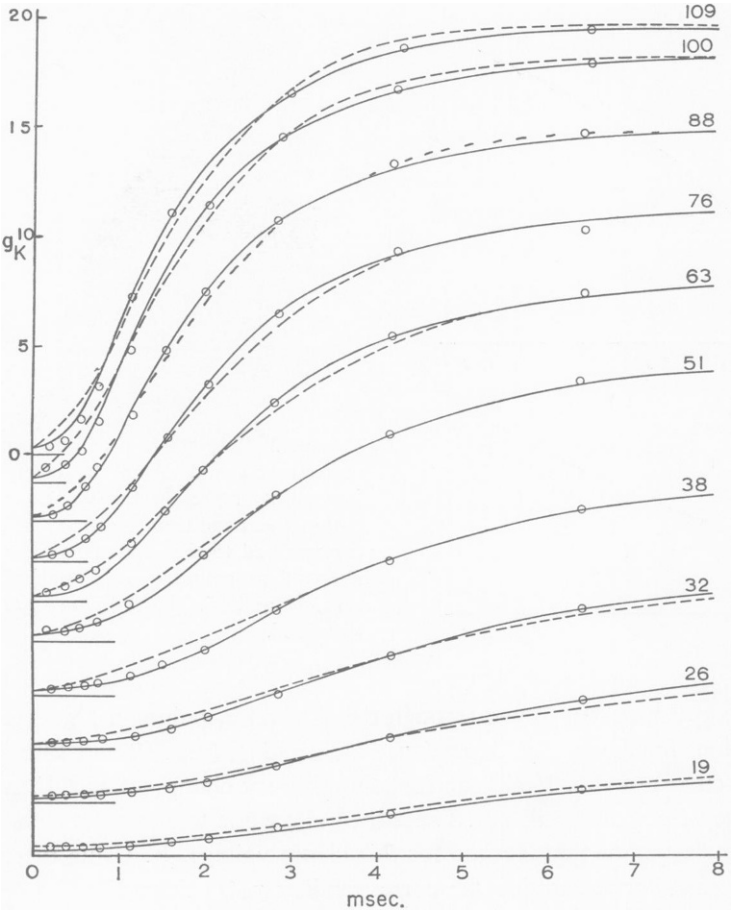

FIGURE 4 Time dependence of the potassium conductance during depolarizing voltage clamps. The circles represent the experimental points shown in fig. 3 of HH (2). The solid curves were calculated from the revised model. The dashed curves show the predictions of the original HH model. The numbers at the right of each curve give the value of the clamp in millivolts. The ordinate scale is in mmho/cm^2; it applies to each curve.

ing potential, such log-log curves for different fibers, and at different temperatures, can be quite closely superimposed by merely adjusting the values t_0 and τ. Cole and Moore showed in this way (*cf.* their fig. 2) that such data can be better represented by a 6th power law than the 4th power law of HH (2). Fig. 5 shows the results of a comparison between the results predicted by a 6th power law and those predicted by the curve of Fig. 2. Considering the scatter shown by the experimental points in fig. 2 of Cole and Moore the two models can be considered as giving equally good fits to the data. One is therefore justified in assuming that the form of the de-

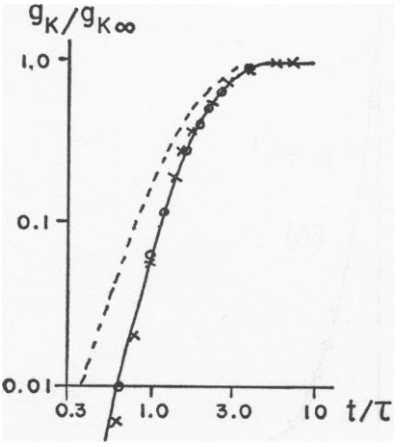

FIGURE 5 Time dependence of g_K during a depolarizing clamp to near the sodium potential. The crosses, ×, are calculated by the present model for a clamp of 109 mv, while the circles, ○, are the HH experimental points for the 109 mv case. The dashed curve corresponds to the HH fourth power law, and the solid curve to the sixth power law of Cole and Moore.

pendence of g_K on v_k, shown in Fig. 2, is approximately the same for all squid fibers under normal ionic conditions and over temperature ranges of 5°C to 20°C.

No test of generality similar to that used above for the $g_K(v_k)$ curve has as yet been made on the variation of the parameters a_k and $v_{k\infty}$ with membrane voltage. (The temperature coefficient of $Q_{10} = 3$, found by Hodgkin, Huxley, and Katz (8), should of course apply to the parameter a_k shown in Fig. 3*b*.) The smooth curves shown in Fig. 3 were not drawn according to any particular analytic forms and were inserted only to aid the eye in estimating the functional behaviors. In order that membrane action potentials could be computed during the "positive after-potential," extrapolations up to hyperpolarizations of 10 mv have been estimated. However no attempt has as yet been made to obtain extrapolations up to the large hyperpolarizations used by Cole and Moore (1). The ability of the present model to give the large delays found by Cole and Moore under such hyperpolarizations will be discussed in the last section.

The above presentation has been restricted to the mathematical model used for potassium conductance, without consideration of any physicochemical model that may lie behind it. A discussion of a possible physical model that may lie behind this mathematical model is given in Appendix III.

With the $g_K(v_k)$, $v_{k\infty}(V)$ and $a_k(V)$ curves determined from the experimental clamp data, it is possible to predict the behavior of the potassium conductance under other conditions. For example, repolarization curves have been calculated, using the extrapolated value of a_k (0) = 0.316 msec. Typical results are shown in curves *a* and *b* of Fig. 6. Since HH found that the decay of g_K upon repolarization was quite closely given by a simple exponential (HH, 10), semilog plots of the calculated fall of g_K were made and, as the examples of Figs. 6*c* and *d* show, the predicted behavior according to the present model is indeed exponential except at very large and very small values of g_K.

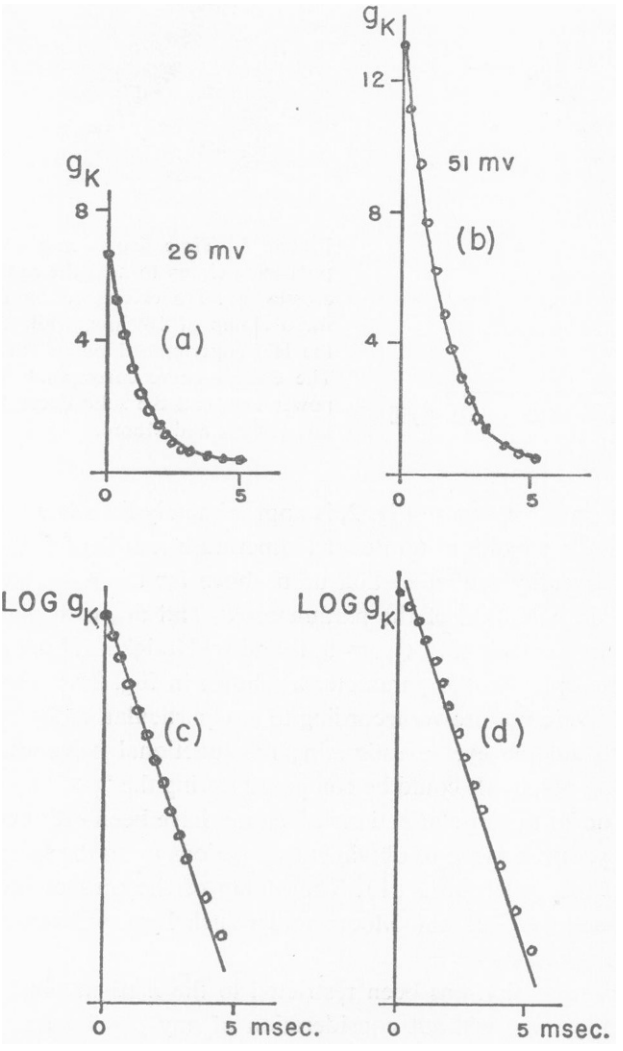

FIGURE 6 Calculated behavior of the potassium conductance during repolarization to the resting potential. The conductance values at the start of curves *a* and *b* are those attained during long lasting depolarizing clamps of 26 mv and 51 mv, respectively. The conductance scale is in mmho/cm^2.

THE SODIUM CONDUCTANCE

Single Voltage Clamp. Under a depolarizing voltage clamp the sodium conductance, g_{Na}, rises, with a short initial delay, up to a maximum and then decreases to a final equilibrium value that may be only slightly above the initial level. This behavior was obtained in the HH mathematical model by assuming that g_{Na} is directly proportional to the product of the third power of a variable m and the first

power of a variable h. Under a depolarizing clamp m is assumed by HH to increase exponentially with time from a very small resting value to a final equilibrium value m_∞, while h decreases exponentially from an initial value h_0 to a very small final value.

In the present model, g_{Na} is assumed to depend explicitly on *one* variable only, v_N, instead of the two variables of HH (2). If the dependence of g_{Na} on v_N, $g_{Na}(v_N)$, is a monotonically rising one, similar to the $g_K(v_k)$ curve, the rise and fall of g_{Na} will result if $v_N(t)$ itself rises and then falls. This behavior of v_N can be obtained if it is assumed that v_N satisfies a second order differential equation rather than a first order one, thus

$$\ddot{v}_N + \gamma \dot{v}_N + \delta[v_N - v_N(\infty)] = 0 \tag{3}$$

where $v_N(\infty)$ is the equilibrium value that v_N approaches at the particular clamp voltage used, and γ and δ are voltage-dependent parameters.

As in the potassium case the zero of v_N will for convenience be taken at the normal resting equilibrium state of $V = 0$. For single clamps starting from the resting membrane voltage, the initial value of v_N is then $v_N(0) = 0$, and the solutions to Eq. 3 have the form

$$v_N = A(1 - e^{-at}) - B(1 - e^{-bt}) \tag{4}$$

where the final equilibrium value of v_N is given by $v_N(\infty) = A - B$, and the initial rate of change of v_N is given by $\dot{v}_N(0) = aA - bB$. The coefficients a and b are given in terms of γ and δ as

$$a = [\gamma + \sqrt{\gamma^2 - 4\delta}]/2 \tag{5a}$$

$$b = [\gamma - \sqrt{\gamma^2 - 4\delta}]/2 \tag{5b}$$

In order to apply this model to the $g_{Na}(t)$ clamp curves, the functional dependence of g_{Na} on v_N, is required. The procedure used to deduce the shape of the $g_{Na}(v_N)$ curve is outlined in Appendix II, and the resulting empirically determined curve is shown in Fig. 7. The parameters $v_N(\infty)$, $\dot{v}_N(0)$, γ and δ were chosen, in conjunction with this $g_{Na}(v_N)$ curve, to give the best fit to the experimental results of HH for axon 17 (fig. 6 of HH, 2). The values so chosen for these parameters, for each different clamp voltage, are shown in Fig. 8. The computed $g_{Na}(t)$ clamp curves are shown by the solid curves in Fig. 9. Where there was a deviation between the curves of the present model and those of HH, the latter are shown by the dashed curves. It can be seen that the present model gives a fit to the experimental points that is equally as good as that of the HH model. (As in the potassium case it should be noted that the ordinate of Fig. 7 should be multiplied by a factor of about 1.6 in order to give results more typical of an average axon in good condition).

In this model then, the $g_{Na}(v_N)$ curve of Fig. 7 replaces the HH equation, $g_{Na} = \bar{g}_{Na} m^3 h$, while the second order differential equation for v_N, (Eq. 3), replaces the

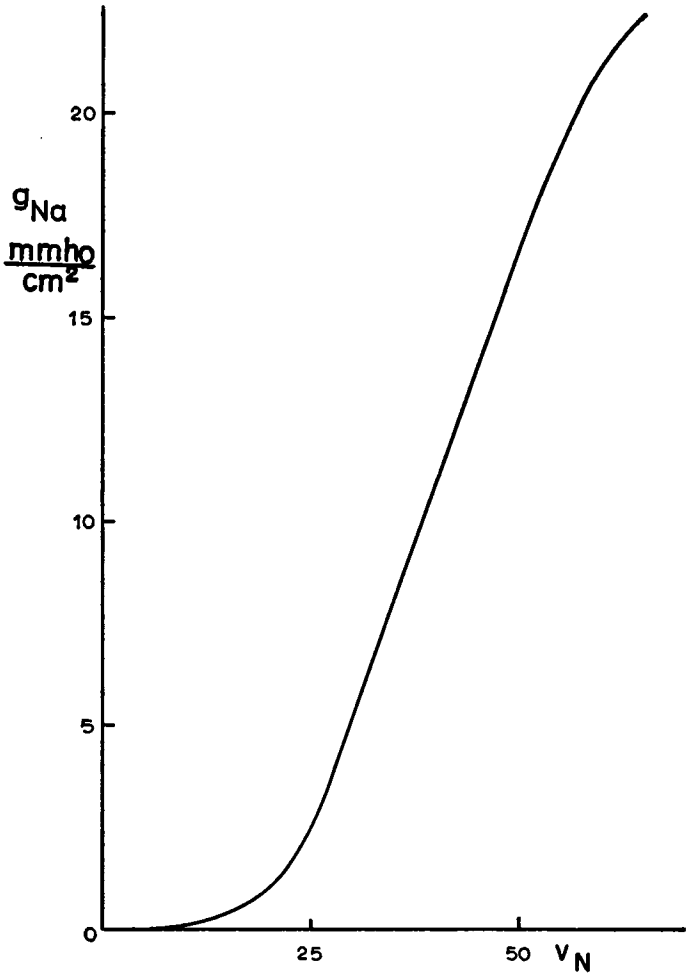

FIGURE 7 Dependence of the sodium conductance on the variable v_N.

two HH first order equations for m and h. The dependence of the parameters $v_{N\infty}$, $\dot{v}_N(0)$, γ and δ on the clamping voltage, shown by the smooth curves drawn to approximate the empirically determined points in Fig. 8, replace the four HH equations giving the voltage dependence of the parameters α_m, β_m, α_h and β_h in the HH model. For any arbitrary clamping voltage, V, the behavior of $g_{Na}(t)$ can be predicted by (a) reading off of the curves of Fig. 8 the values of the parameters $v_{N\infty}$ etc., (b) using these in Eq. 4 to determine the variation of v_N with time, and (c) using these $v_N(t)$ values together with the $g_{Na}(v_N)$ curve of Fig. 7 to determine the desired $g_{Na}(t)$ clamp curve (see Fig. 22 in Appendix II).

Generalization of the v_N Equation. The mathematical model for the sodium conductance presented above has been shown to be able to account satis-

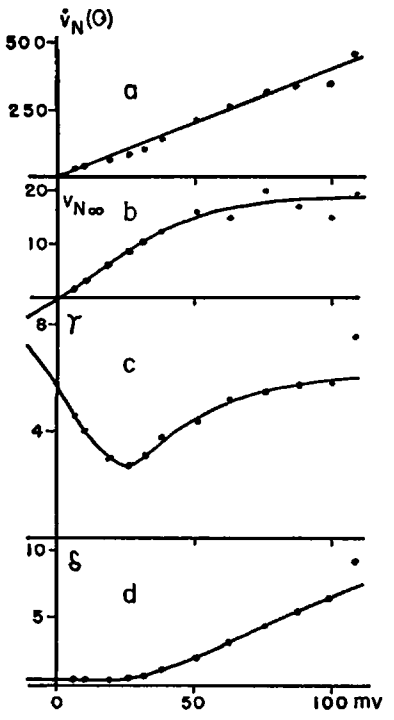

FIGURE 8 Dependence of the sodium parameters on the clamping voltage. The points represent the values used in computing the conductance curves of Fig. 9. The ordinate scales are in $(\text{msec.})^{-1}$ for $\dot{v}_N(0)$ and γ, and in $(\text{msec.})^{-2}$ for δ.

factorily for the results of a simple deplorizing clamp that starts from the resting membrane potential. The extent to which such a model can be modified to include other phenomena, such as the effects of conditioning clamps and the behavior when the voltage varies with time, will now be discussed.

In the Hodgkin and Huxley model, the sodium conductance is a function of two variables m and h, each of which satisfy first order differential equations, with coefficients that are functions of the membrane voltage. The two variables m and h act independently of each other, and are not considered to be coupled in any way. In the present model the sodium conductance is assumed to depend explicitly on only one variable, this one variable satisfying, under clamp conditions, a second order differential equation. When one considers how such a second order equation may arise a reasonable hypothesis is that it results from two *coupled* first order equations.

A number of different pairs of coupled equations could be written down, but only one case, simple enough so that it can be completely analyzed, will be treated here. It should be considered as an example only, and not necessarily as the case that gives the best fit to the data.

The pair of coupled equations that have been investigated are

$$\frac{du}{dt} = -k_1 u + k_2 \tag{6a}$$

$$\frac{dv}{dt} = k_1 u - k_3 v + k_4, \tag{6b}$$

where the rate constants (k_1, k_2, k_3, k_4) are assumed to be functions of the membrane voltage. The variable u can be eliminated between the two equations, leading to an equation for v alone:

$$\ddot{v} + (k_1 + k_3)\dot{v} + k_1 k_3 \left[v - \left(\frac{k_2 + k_4}{k_3} \right) \right] = \left[u \frac{dk_1}{dV} - v \frac{dk_3}{dV} + \frac{dk_4}{dV} \right] \dot{V}. \tag{7}$$

Identifying v with v_N, it is seen that Eq. (7) reduces to the form of Eq. (3) for the case of a constant, clamped voltage (*i.e.* $\dot{V} = 0$), with

$$\gamma = k_1 + k_3 \tag{8a}$$

$$\delta = k_1 k_3 \tag{8b}$$

$$v_{N\infty} = (k_2 + k_4)/k_3. \tag{8c}$$

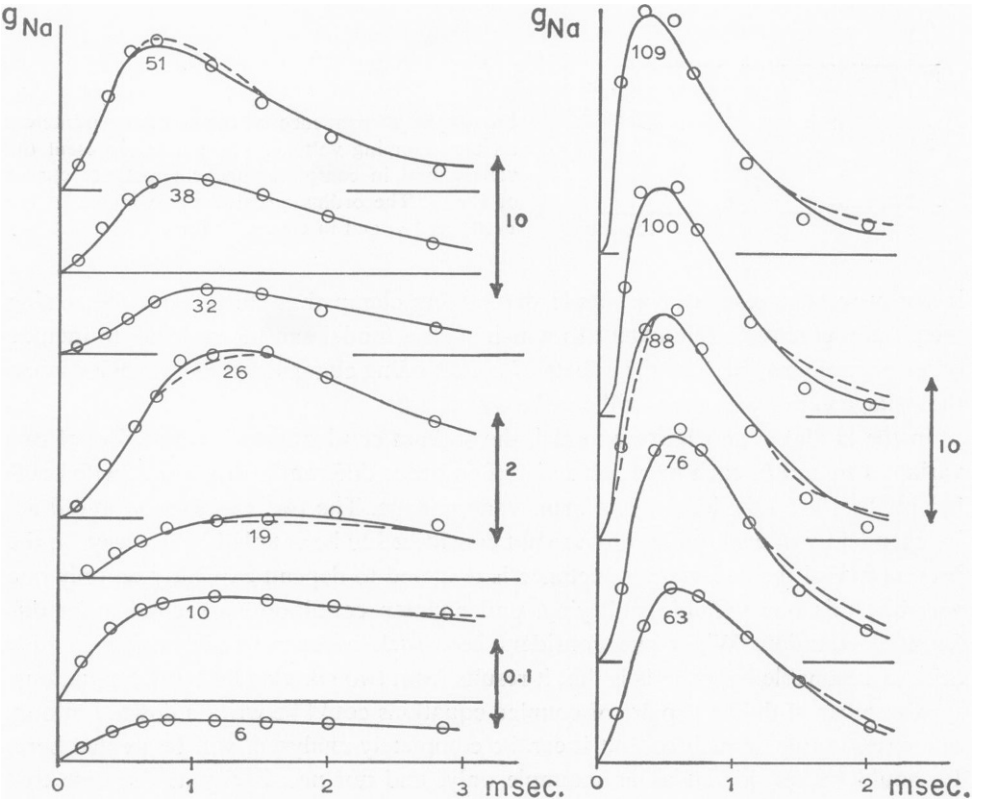

FIGURE 9 Time dependence of the sodium conductance during depolarizing clamps. The circles represent the experimental points shown in fig. 6 of HH (2). The solid curves were computed by the present model. The dashed curves show the predictions of the HH model. The numbers associated with each curve give the value of the clamp in millivolts. The vertical lines show the ordinate scales in mmho/cm^2.

Choosing the origin for u, as well as that of v_N, at the resting potential, one has for a clamp starting from the resting potential

$$\dot{v}_N(0) = k_4. \tag{8d}$$

As will be shown below, the four equations $8(a - d)$ are sufficient to determine the four rate constants (k_1, k_2, k_3, k_4), as functions of the membrane voltage. Knowledge of these four rate constants will then allow predictions to be made of the behavior of v_N (and thus of g_{Na}) in the case of (a) a test clamp following a conditioning clamp, (b) recovery following a rectangular test pulse, (c) the behavior of v_N during repolarization, and (d) the calculation of action potentials and other phenomena involving time varying potentials.

Solving Eqs. ($8a$) and ($8b$) for k_1 and k_3 in terms of γ and δ one obtains

$$k_1 = [\gamma \pm \sqrt{\gamma^2 - 4\delta}]/2$$
$$k_3 = [\gamma \mp \sqrt{\gamma^2 - 4\delta}]/2.$$

Upon comparing these with Eqs. ($5a$) and ($5b$), it is seen that either $k_1 = a$ and $k_3 = b$, or $k_1 = b$ and $k_3 = a$. It is found that the first choice leads to results in agreement with the HH experimental results on inactivation, HH (11), while the second choice does not. Using the first choice, the values of the rate constants then become

$$k_1 = a \tag{9a}$$
$$k_2 = bv_{N\infty} - \dot{v}_N(0) \tag{9b}$$
$$k_3 = b \tag{9c}$$
$$k_4 = \dot{v}_N(0). \tag{9d}$$

Using the values of a, b, $v_{N\infty}$ and $\dot{v}_N(0)$, previously determined to give the best fit to the clamp data, the values of k_1, k_2, k_3 and k_4 have been computed as functions of the membrane voltage and the results are shown in Fig. 10. Extrapolated values for hyperpolarizing voltages up to 10 mv are shown by the dashed extensions of the curves. For some of the effects computed below, the equilibrium values of u_N are required.[3] These are given by $u_{N\infty} = k_2/k_1$. The computed values of $u_{N\infty}$ are plotted in Fig. 10, together with those previously determined for $v_{N\infty}$.

Inactivation, Recovery, Repolarization. In each of the cases treated in this section it is necessary to compute the time course of v_N under clamped voltages but with the initial conditions not those applying for a clamp starting from the resting state [*i.e.* $v_N(0) = u_N(0) = 0$ and $\dot{v}_N(0) = k_4$]. Rather the initial conditions are $v_N(0) = v_{N0}$, $u_N(0) = u_{N0}$ and $\dot{v}_N(0) = k_1u_{N0} - k_3v_{N0} + k_4$. The dependence of v_N on time is then given by

$$v_N = C_1 + C_2e^{-at} + C_3e^{-bt}, \tag{10}$$

[3] From here on u will be denoted by u_N.

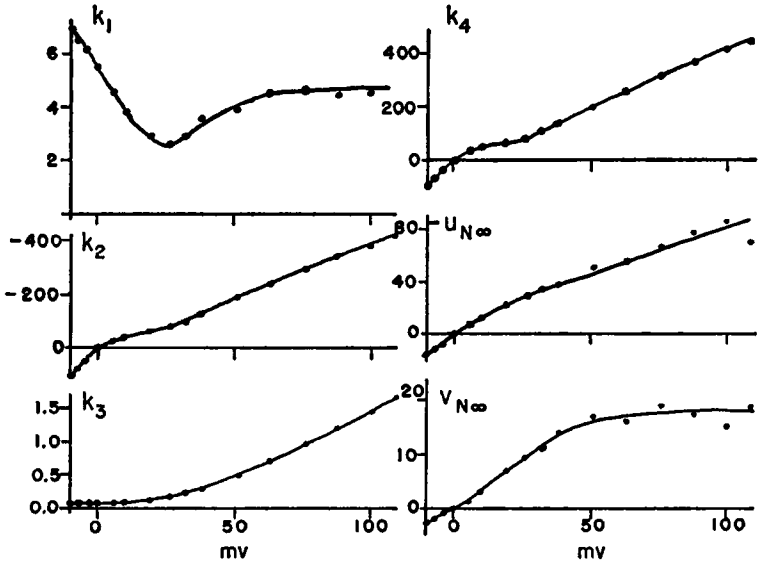

FIGURE 10 Variation with membrane voltage of the parameters of the coupled equations model. The ordinate scales for k_1, k_2, k_3, and k_4 are in (msec.)$^{-1}$. *Note* that k_2 and $u_{N\infty}$ are both negative for depolarizing (+) voltages.

where the constants C_1, C_2 and C_3 are given in terms of the initial conditions by

$$\begin{aligned} C_1 &= v_{N\infty} \\ C_2 &= -[\dot{v}_N(0) + b(v_{NO} - v_{N\infty})]/(a - b) \\ C_3 &= \quad [\dot{v}_N(0) + a(v_{NO} - v_{N\infty})]/(a - b) \end{aligned} \tag{11}$$

Once the time course of v_N has been computed the time course of g_{Na} can then be determined from the $g_{Na}(v_N)$ curve of Fig. 7.

The effect of a long lasting conditioning clamp on the maximum change of g_N during a succeeding test clamp has been computed using the method outlined above. The results are shown Fig. 11*a* and it is seen that the agreement with fig. 5 of HH (11) is excellent. One computation has also been made of the time course of the development of "inactivation" and the results are shown in Fig. 11*b*. Here too the agreement with the experimental results of HH are also excellent (*cf.* fig. 3 of HH (11)). In the model being used the inactivation effect is due to the reduction in $\dot{v}_N(0)$ at the start of the test clamp. From Eq. (6*b*) it is seen that starting from the resting state, where $u_N(0) = v_N(0) = (0)$, the initial velocity is given by $\dot{v}_N(0) = k_4$. However at the start of a test clamp which is preceded by a conditioning clamp, $v_N(0) > 0$ and $u_N(0) < 0$, and both of the first two terms in Eq. 6*b* act to reduce the initial velocity, *i.e.*, $\dot{v}_N(0) < k_4$. This reduction in $\dot{v}_N(0)$ in turn leads to a reduction in the maximum value attained by v_N during the test clamp, and thus to the maximum value attained by g_{Na}.

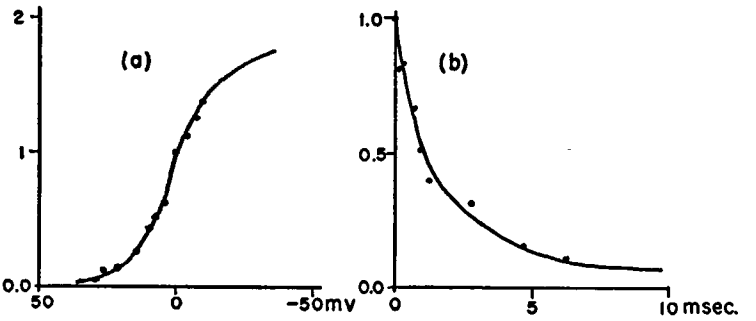

FIGURE 11 "Inactivation" due to conditioning pre-clamps. The ordinates in both (*a*) and (*b*) represent the ratio of the maximum g_{Na} attained during the (44 mv) test clamp to that attained in an unconditioned (44 mv) test clamp. (*a*) The effect of long lasting conditioning pre-clamps (steady state). The abscissa represents the size of the conditioning clamp in millivolts. Note that deplorizing (+) voltages are plotted to the left, hyperpolarizing (—) voltages to the right. The points represent the results computed from the curves of Figs. 7 and 10. (*b*) The time development of "inactivation" for a (depolarizing) conditioning clamp of 29 mv.

Calculations have also been made to determine the maximum value attained by v_N (and thus by g_{Na}) in the second test pulse in the two pulse experiment of fig. 6 of HH (11). The results are shown in Fig. 12, and are seen to be in substantial agreement with the experimental results of fig. 7 of HH (11). The apparent time constant of this recovery curve is 13 msec., in good agreement with the value of 12 msec. obtained experimentally by HH.

Finally, the time course of g_{Na} during repolarization to the resting potential has been computed with the results shown in Fig. 13. Here too the results are in substantial agreement with the experimental results of HH (*cf.* fig. 10 of HH (10)),

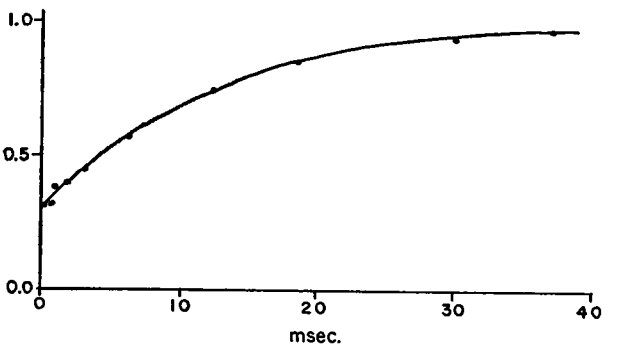

FIGURE 12 Recovery from the "inactivation" due to a prepulse of 44 mv lasting for 1.86 msec. The ordinate represents the ratio of the maximum g_{Na} attained during the 44 mv test pulse to that attained in an unconditioned, 44 mv, test pulse. The abscissa represents the interval between the end of the first pulse and the beginning of the second pulse. The points represent the results computed from the curves of Figs. 7 and 10.

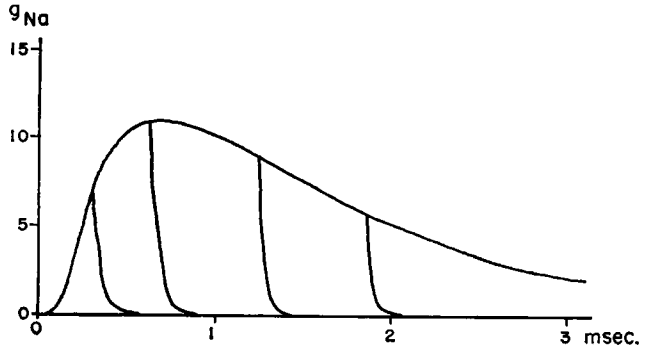

FIGURE 13 The effect of repolarization on the time course of g_{Na}. The continuous curve represents the computed behavior of g_{Na} during a clamp of 51 mv. The computed effect of repolarizing the membrane to its resting voltage is shown for various times after the start of the clamp. The ordinate scale is in mmho/cm^2.

except that g_{Na} falls somewhat more rapidly in the computed curves than in the HH experimental case.

MEMBRANE ACTION POTENTIALS

Further checks on the validity of the mathematical models suggested above for the potassium and sodium conductances can be obtained by investigating the degree to which they can jointly account for the many additional phenomena of nerve behavior such as action potentials, refractory period, subthreshold responses, etc. Preliminary calculations of "membrane" action potentials have been made and the results are presented below.

In the measurement of non-propagated "membrane" action potentials, the potential is kept uniform over a long length of the fiber and is measured with an instrument of very high input inpedance. Therefore, except during the shock stimulus, the net membrane current can be considered to be zero. Using the equivalent circuit of Fig. 1, the equation for the membrane potential V is then (*cf.* eq. 26 of HH (2)),

$$I = 0 = C_M \frac{dV}{dt} + (V - V_K)g_K + (V - V_N)g_{Na} + (V - V_L)g_L, \qquad (12)$$

with the initial condition of $V(0) = V_0$, the voltage to which the membrane is raised by the shock stimulus.

Note that all potentials are measured relative to the resting membrane potential. Thus, if E is the instantaneous absolute membrane potential difference and E_R the resting potential difference, we have $V = E - E_R$. The net driving voltage for potassium ions is $V - V_K$, where $V_K = E_K - E_R$; here E_K is the potassium EMF due to the concentration difference of potassium ions on the two sides of the membrane. Similar expresions hold for the sodium ions and for the leakage effect (L) of all other ions.

According to the models for the sodium and potassium conductances discussed in the preceding sections, g_K and g_{Na} are to be considered functions of the variables v_k and v_N, respectively, as given in Figs. 2 and 7. The variables v_k and v_N are in turn determined by Eqs. (1) and (6*a* and *b*), with the dependence of the parameters on the instantaneous membrane voltage V, being given by the curves of Figs. 3 and 10.

As in the HH treatment, the leakage conductance g_L is assumed to remain constant. This and the other constant parameters are chosen to have the values shown in Table I. As mentioned earlier, the ordinates of Figs. 2 and 7 should probably be

TABLE I

C_M	$= 1.0\mu$ f/cm^2
V_K	$= -12.2$ mv
V_N	$= 115.0$ mv
V_L	$= 10.5$ mv
g_L	$= 0.3$ mmho/cm^2

increased since the conductances for the HH axon 17 are low compared to those for an average axon. This was not, however, done for the first set of membrane action potentials computed. The effect of increasing the ordinates was later tested in one case.

Numerical integrations of Eq. 12 lead to the computed membrane action potentials shown in Fig. 14. Comparison with the curves of fig. 12 of HH (2) shows that the curves calculated by the present K and the Na models are reasonably satisfactory except that the falling phase is perhaps a little too rapid. In particular, it is seen that the present models are, like the HH models, able to predict the presence

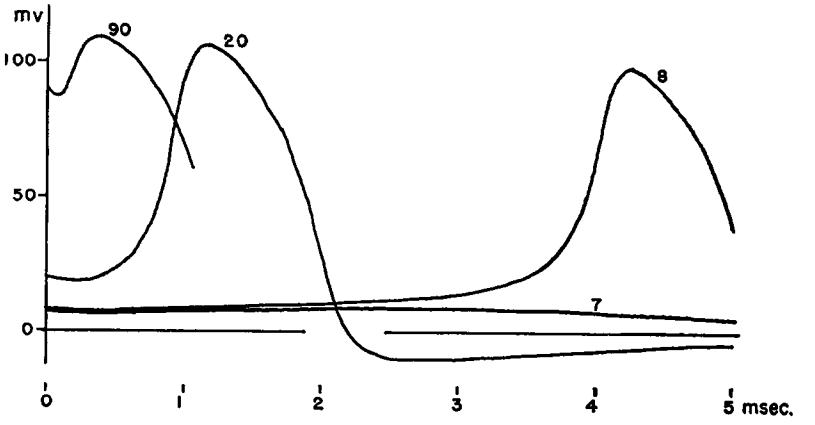

FIGURE 14 Computed membrane action potential curves. The numbers associated with each curve represent the voltage level, in millivolts, by which the membrane is supposed to be instantaneously displaced by a shock stimulus.

of a threshold. The computed conductance changes accompanying the action spike are shown for one action potential in Fig. 15*a*. Other than the expected result that the maximum magnitude attained by the conductance is smaller than expected for a normal fiber, the curve is very similar to that computed by HH and also similar to that experimentally found by Cole and Curtis (*cf.* fig. 16 of HH (2)). The effect of increasing all conductances by a factor of 1.6 was tested for one case, with the result shown in Fig. 15*b*. It is apparent that the form of the curves for the action

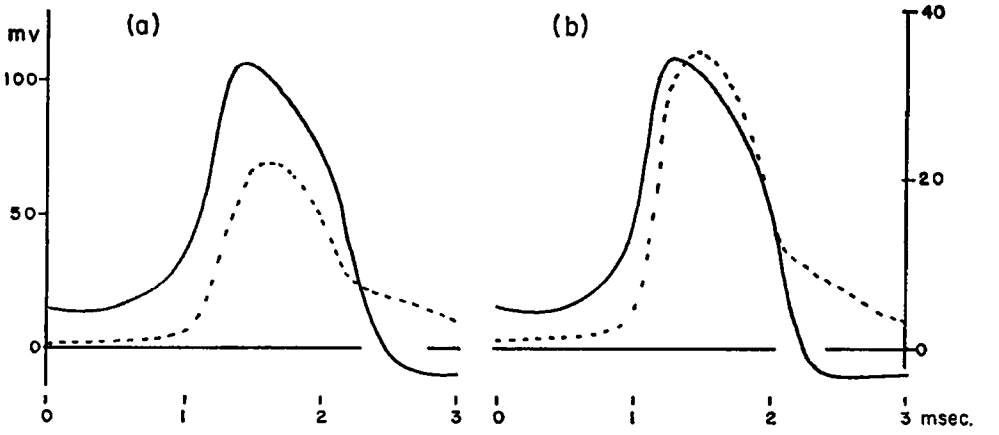

FIGURE 15 (*a*) Computed membrane action potential curve (solid) and total membrane conductance curve (dashed) for an initial voltage displacement of 15 mv. The left-hand ordinate refers to the solid curve. The right hand ordinate refers to the dashed curve, and its scale is in mmho/cm². (*b*) Same as (*a*) except the ordinates in Figs. 2 and 7 were multiplied by 1.6 before being used. Likewise the g_L value given in Table I was multiplied by 1.6 (*i.e.* $g_L = 0.48$ mmhos/cm²).

potential and total conductance are very little changed, but that the maximum value attained by the conductance is now in agreement with the results of fig. 16 of HH (2).

DISCUSSION

Potassium Conductance. Cole and Moore (1) have investigated the behavior of the potassium conductance for clamps close to the sodium potentials. They have found that, over a wide range of preclamping voltages, the resulting time curves can be brought into coincidence by simple translations along the time axis. As indicated by the authors, this behavior would seem to suggest that g_K depends on a single variable, and that this variable satisfies a first order differential equation.

Both the model based on the $g_K(v_k)$ curve of Fig. 2 and the power law models of HH and of Cole and Moore assume first order behavior for the time dependent variable and thus satisfy the above criterion. The power law assumption is attractive

because of its simplicity and because of its simple interpretation in terms of the probability of finding a given activating agent at a specific membrane site. Yet these attractions do not rule out the possibility that it may be some other type of functional dependence that is involved. It would now seem from the results presented earlier that the relationship given in Fig. 2 gives a better fit for clamps starting from the resting potential than does the HH fourth power law, and gives as good a fit as the higher order power law assumed by Cole and Moore.

The major reason for Cole and Moore's choice of a 25th power was to account for the very considerable time delays observed with large hyperpolarizing preclamps. In the present model, clamps starting at other than the resting state will do so from an initial value of $v_k = v_{k0}$ that is not zero. The solution to Eq. (1) then becomes

$$v_k = v_{k\infty}\left[1 - \frac{v_{k\infty} - v_{k0}}{v_{k\infty}} e^{-\alpha_k t}\right]$$

where v_{k0} will be negative for hyperpolarizing preclamps. This can be put in the form

$$v_k = v_{k\infty}[1 - e^{-\alpha_k(t-t_0)}]$$

were t_0 is the time delay caused by the preclamp. In the power law models it is assumed that the minimum allowable value for the variable n is zero, and this restricts the maximum allowable delay time, t_0. In the present model, no physical interpretation has as yet been given to the variable v_k and the extrapolation of the curve of Fig. 3*a* can be made to give large negative values of $v_{k\infty}$. Very large delays are thus mathematically possible. It is to be assumed, however, that the physical system that lies behind the mathematical model will put a limit on how large a negative value v_k can take on. It is, of course also to be assumed that the $g_K(v_k)$ values remain positive for all allowable negative values of v_k.

It is shown in Appendix III that the $g_K(v_k)$ curve of Fig. 2 can be given a simple physical interpretation. Using this interpretation estimates of the minimum and maximum values of v_k can be made leading to -90 and $+171$, respectively (analogous to the 0 and 1 limits of the Hodgkin and Huxley variable n). This model then leads, for a clamp to the sodium potential, to a maximum delay of about 1 msec. between a clamp that starts at the resting potential and one that starts at a large hyperpolarization. The above calculation assumes a fiber temperature of 6°C. Using the temperature coefficient of 3 that was found by HH, the maximum delay at 20°C becomes 0.21 msec., in good agreement with the results shown in fig. 5 of Cole and Moore (1).

Sodium Conductance. As indicated earlier, although the model being considered here for the sodium conductance depends explicitly on only one variable, the second order differential equation that this variable is assumed to satisfy is most easily considered as resulting from the coupling of two variables, as in Eqs. (*6a* and *b*). Such a pair of coupled variables suggest quite different physicochemical

mechanisms than do the pair of non-coupled variables used by HH (2). Mathematically the coupled and non-coupled models can lead to quite similar though not necessarily identical results under any one set of environmental conditions. By changing the environmental conditions, such as with TEA treatment (3–5), it may be possible to distinquish the two mathematical types experimentally, though this may be difficult. A more worthwhile approach might be to consider the types of physicochemical systems that may lie behind the two types of mathematical models. Maybe specific biochemical and biophysical experiments can then be devised to test for specific effects suggested by these physicochemical models.

The physical model suggested by Mullins (12) bears some mathematical similarity to the one suggested here. In the Mullins model the sodium conductance of the membrane is assumed to depend primarily on one variable only, namely the number of pores that are both unblocked and are of the proper "sodium size." Further, the value of this one variable depends on the coupling of two processes, namely the unblocking of the pores and the subsequent inactivation due to a change of size of the unblocked pores. However, the Mullins model assumes that the delayed rise in potassium conductance results from the same process that causes the sodium inactivation. Such an additional coupling between the sodium and potassium mechanisms has not been assumed here since it would imply that the variable responsible for the potassium conductance changes does not satisfy a first order equation contrary to the evidence presented by Cole and Moore (1). Further it would predict a connection between the time constants for the sodium conductance changes and those for the potassium conductance changes, and no such connection is experimentally evident.

The pair of coupled equations given in Eqs. (6*a* and *b*) are a special case of the more general equations

$$\frac{du}{dt} = -k_1 u + k_2 v + k_3$$

$$\frac{dv}{dt} = -k_4 v + k_5 u + k_6. \tag{13}$$

The discrepancies so far noted (the greater rapidity of the computed as opposed to the experimentally observed fall of g_{Na} with repolarization and falling phase of the action potential) may indicate that the case chosen for analysis is oversimplified and that a more general case of Eqs. (13) should be tried. However, the discrepancies so far noted are minor, and it does not seem profitable at the moment to go to the added complexity of five or six rate constants instead of the four present in the case of Eqs. (6*a* and *b*). The general case of Eqs. (13) can be fitted to a wide variety of different physical and chemical systems; for example, dipole systems of the type considered in Appendix III, but with three stable orientations rather than two, only one of which represents sodium activation. Another example is a system of coupled

chemical reactions such as the Nachmanson hypothesis (15) in which acetyl choline is released from a storage protein, combines reversibly with a receptor protein and is destroyed by esterase.

APPENDIX I—g_K

1. *Determination of the $g_K(v_k)$ Curve*

The method used to determine empirically the shape of the $g_K(v_k)$ curve consisted of making an initial guess and then using the results of this guess as the starting point for a successive approximation procedure.

(*a*) The first guess (approximation) consisted of the assumption that the final equilibrium value of v_k, $v_{k\infty}$, is proportional to the clamping voltage V. Making this assumption, and choosing the scale for v_k so that $v_{k\infty} = V$, the first approximation curve, $g_K(v_{k1})$ of Fig. 16*a* was then obtained by plotting the final equilibrium values of g_K, $g_{k\infty}$, against the clamp voltage V. This first approximation was tested by using the experimental $g_K(t)$ curve for a clamp of 100 mv and reading off of Fig. 16*a* the corresponding $v_{k1}(t)$

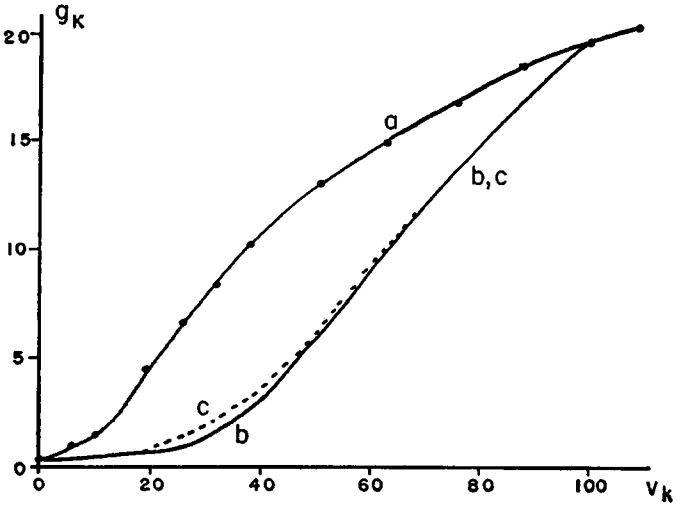

FIGURE 16 Successive approximations to the $g_K(v_k)$ curve. The ordinate scale is in mmho/cm².

values. A semilogarithmic plot of $v_{k1}(\infty) - v_{k1}(t)$ was made, with the results shown in Fig. 17*a*. If the original assumption (that $v_{k\infty} \propto V$) were correct, the points plotted in Fig. 17*a* should lie on a straight line. The very considerable divergence from a straight line indicates that the first approximation is far from correct. However, the fact that one portion of the log curve is well fitted by a straight line would seem to indicate that the original assumption, of a linear relation between $v_{k\infty}$ and V, is indeed correct over this limited region.

(*b*) The second approximation was obtained by using the straight line portion of Fig. 17*a*. Thus it was assumed that for $V = 100$ mv, v_k is given by

$$v_k = A(1 - e^{-\alpha t})$$

where A was arbitrarily taken to be 100 and a, determined from the slope of the straight line portion of Fig. 17*a*, is given by $a = 0.63$ msec. The resulting computed values for $v_k(t)$ were then used in conjunction with the experimental $g_K(t)$ clamp curve for $V = 100$ mv to obtain the second approximation for the $g_K(v_k)$ curve. The resulting curve is shown in Fig. 16*b*.

The second approximation curve of Fig. 16*b* was checked by using it, together with the experimental $g_K(t)$ clamp curve for $V = 51$ mv, to obtain values for $v_k(t)$ at 51 mv. The resulting semilogarithmic plot is seen to approximate, closely but not exactly, a straight line (Fig. 17*b*).

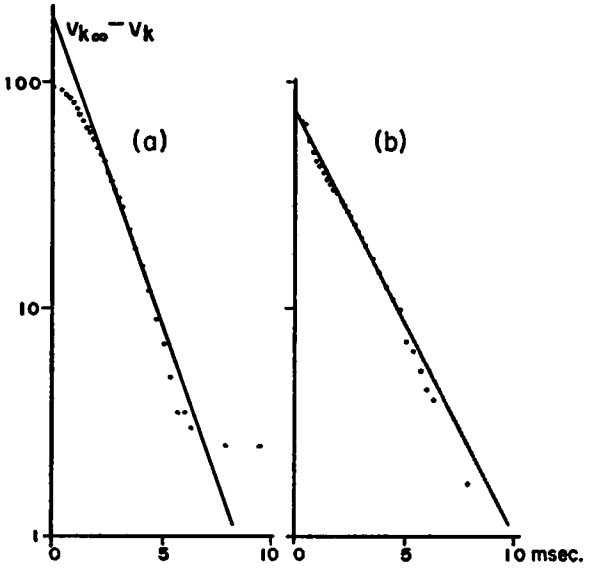

FIGURE 17 (*a*) Semilogarithmic plot of $v_{k\infty} - v_k$ against time, obtained using the experimental $g_K(t)$ clamp for 100 mv and curve (*a*) of Fig. 16. (*b*) Semilogarithmic plot of $v_{k\infty} - v_k$ against time, obtained using the experimental $g_K(t)$ clamp for 51 mv and curve (*b*) of Fig. 16.

(*c*) The third approximation was obtained by assuming that $v_k(t)$ for 51 mv follows the straight line of Fig. 17*b*. Using this assumption the $g_K(v_k)$ curve of Fig. 16*c* was obtained. Using this revised $g_K(v_k)$ curve, a recheck showed that the computed $V = 100$ mv clamp still gave a good fit to the experimental data.

(*d*) The procedure outlined above was pursued for several other clamp voltages, leading in each case only to minor revisions of the $g_K(v_k)$ curve, revisions which improved the predicted behavior for some clamps and left others essentially unchanged. The final curve chosen follows curve (*c*) so closely that the differences are undetectable on the scale to which Fig. 16 is drawn. The final curve itself is shown in Fig. 2 (note that the scales have been changed). Using this final curve, readjustments were made in the $v_{k\infty}$ and a_k values for each clamping voltage to give the best fit of each clamp curve. These final $v_{k\infty}$ and a_k values are shown in Fig. 3, while the clamp conductance curves are shown in Fig. 4.

2. *Prediction of $g_K(t)$ under a Voltage Clamp*

The curves of Fig. 2 and Fig. 3 were chosen to give fits to the specific clamp data of fig. 3 of HH (2). They can of course also be applied to the computation of any clamp. For example, from the curves of Fig. 3 it is predicted that for a clamp of 70 mv the values of a_k and $v_{k\infty}$ should be 5.0/msec. and 84.8 respectively. For a clamp to 70 mv, starting from rest, the behavior of v_k should then be given by

$$v_k = 84.8[1 - \exp(-5.0t)].$$

A plot of this equation is given in Fig. 18*a*.

For each $v_k(t)$ value the corresponding g_K value can be read off of the curve of Fig. 2. The resulting predicted clamp curve for 70 mv is shown in Fig. 18*b*.

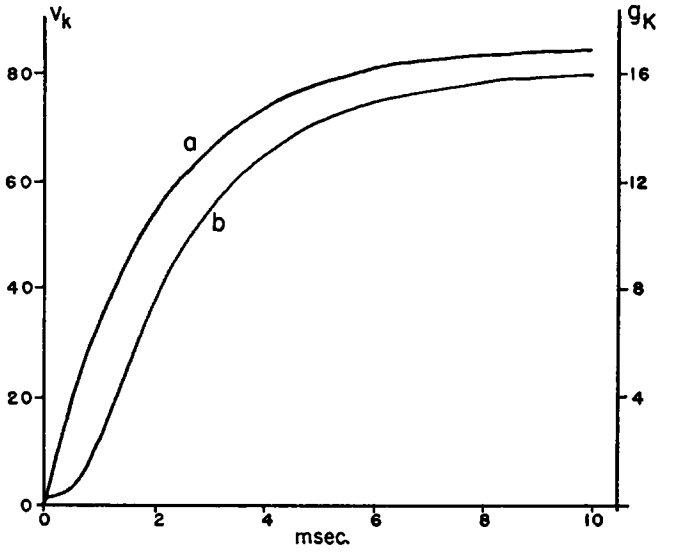

FIGURE 18 Predicted variation of v_k and g_K as a function of time for a clamp of 70 mv. The right-hand ordinate scale, for g_K, is in units of mmho/cm^2.

APPENDIX II—g_{Na}

1. *Determination of the $g_{Na}(v_N)$ Curve*

As in the $g_K(v_k)$ case, the method used to determine empirically the $g_{Na}(v_N)$ curve consisted of making an initial guess and then using the results of this guess as the starting point of a successive approximation procedure. However, instead of starting with a large clamp as was done in the potassium case ($V = 100$ mv), the curve was determined first for small clamps and was then extended upwards by using successively larger clamps.

(*a*) The first guess (approximation) consisted of the assumption that for small clamps the maximum value attained by v_N, $(v_N)_{max}$, is proportional to the clamping voltage. If this assumption were true then the experimental $(g_{Na})_{max}$ *versus* V curve should also represent the $(g_{Na})_{max}$ *versus* $(v_N)_{max}$ behavior and thus the desired $g_{Na}(v_N)$ curve, to within an arbitrary multiplying constant. The resulting first approximation curve is shown

in Fig. 19*a* for the full range of clamping voltages, although it is only to be expected to have approximate validity over the initial region. This first approximation was tested as follows:

It is assumed that v_N satisfies the second order differential equation of Eq. (3) and thus has solutions of the form given in Eq. (4). It is also assumed that the two constants a and b are considerably different in magnitude, with $b \ll a$. During the falling phase the term e^{-at} will thus become considerably less than the term e^{-bt} and the expression for v_N can be approximated by

$$v_N = v_{N\infty} + Be^{-bt}$$

or,

$$v_N - v_{N\infty} = Be^{-bt},$$

where

$$v_{N\infty} = A - B.$$

The experimental $g_{Na}(t)$ clamp curve for $V = 26$ mv was used in conjunction with the curve of Fig. 19*a* to obtain tentative values of $v_N(t)$. These were then used to plot,

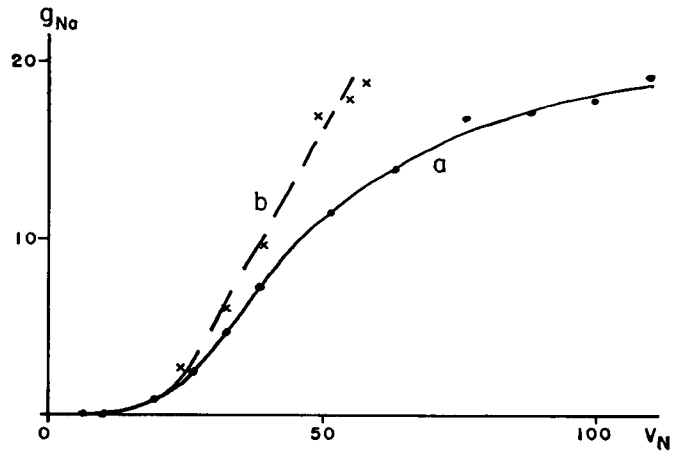

FIGURE 19 Successive approximations to the $g_{Na}(v_N)$ curve. The ordinate scale is in mmho/cm^2.

semilogarithmically, values of $v_N(t) - v_{N\infty}$ where successive values of $v_{N\infty}$ were tried until one ($v_{N\infty} = 4.0$) was obtained that gave a reasonably straight line over the falling phase, as shown in Fig. 20*a*. The slope of this straight line yielded a value of $b = 0.213$/msec., and the intercept yielded the value of $B = 32.6$, while $A = v_{N\infty} + B = 36.6$. The equation for v_N could then be written as

$$36.6e^{-at} = 4.0 + 32.6e^{-0.213t} - v_N.$$

The right-hand side of this equation was then plotted semilogarithmically. The resulting straight line, shown in Fig. 20*b*, indicates that the first approximation yields a self-consistent model over the entire range of the 26 mv clamp. From the slope of this straight line the value of $a = 2.00$/msec. is obtained.

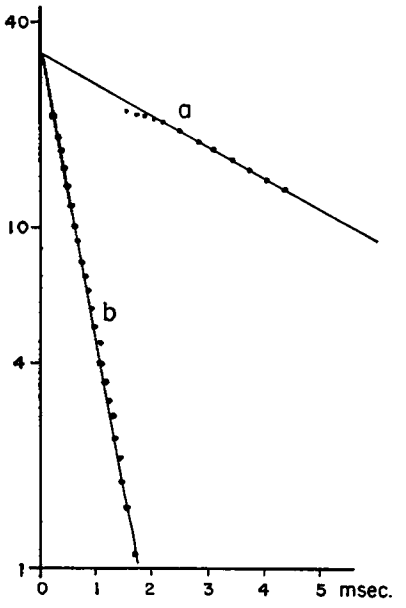

FIGURE 20 (*a*) Semilogarithmic plot of (v_N − 4.0) against time, obtained using the falling phase of the experimental $g_{Na}(t)$ clamp curve for 26 mv and curve (*a*) of Fig. 19. (*b*) Semilogarithmic plot of ($4.0 + 32.6\, e^{-.128t} - v_N$) using the experimental $g_{Na}(t)$ curve for 26 mv and curve (*a*) of Fig. 19.

(*b*) The first approximation curve of Fig. 19*a* was shown above to be satisfactory for a clamp of 26 mv in which the maximum value attained by g_{Na} is about 2.4 mmho/cm^2. However for clamps above 26 mv serious deviations appear, necessitating modifications of the first approximation curve of Fig. 19*a*, as will be shown below.

If the 109 mv clamp is treated in the same way as the 26 mv clamp, it is found that a good fit can be obtained to the latter part of the falling phase and to the initial part of the rising phase, but not for the region in which the g_{Na} values are large. From these initial and final phases of the 109 mv clamp the semilogarithmic plots of Fig. 21 lead to

$$v_N = 16 + 100e^{-1.39t} + 116e^{-5.19t} \tag{14}$$

If it is assumed that Eq. 14 holds over the entire range, the experimental, 109 mv, clamp curve together with this equation lead to new $g_{Na}(v_N)$ values that can be used to correct the curve of Fig. 19*a*. These values are shown by the crosses in Fig. 19, and by the dashed curve (b).

For each of the remaining experimental clamp curves, the curve of Fig. 19*b* was then used to obtain $v_N(t)$ values, and these $v_N(t)$ values were in turn tested to see if they could be adequately fitted to the general equation

$$v_N = A(1 - e^{-at}) + B(1 - e^{-bt}).$$

As a result of these tests, curve (*b*) of Fig. 19 was modified slightly. These modifications are too slight to be indicated in Fig. 19 and the final $g_{Na}(v_N)$ curve, very similar to curve *b* of Fig. 19, is that shown in Fig. 7. After this final curve was obtained each of the clamp curves were refitted to it, with the parameters *A*, *a*, etc., chosen to give the best fit of the computed clamp curves to the experimental data of HH (2). The values of *a* and *b* were then used to determine the parameters $\gamma = a + b$, $\delta = ab$, while the initial rate of rise

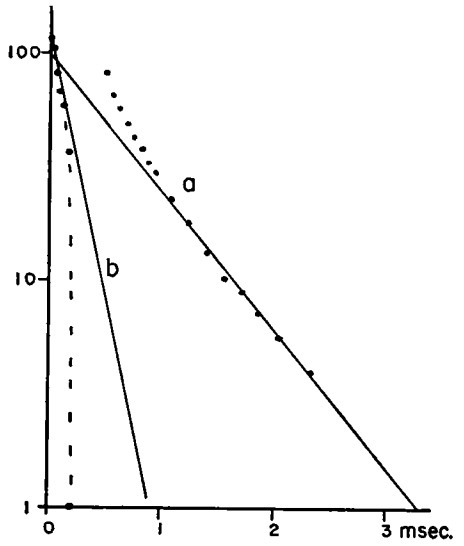

FIGURE 21 (*a*) Semilogarithmic plot of $(v_N - 16)$ against time, obtained using the falling phase of the 109 mv experimental $g_{Na}(t)$ clamp curve and curve (*a*) of Fig. 19. The slope of the straight line yields $a = 5.19$ (msec.)$^{-1}$ and its intercept gives $B = 100$. (*b*) Semilogarithmic plot of $(16 + 116\ e^{-5.19t} - v_N)$ using the 109 mv clamp curve and curve (*a*) of Fig. 19.

of v_N was computed from $\dot{v}_N(0) = aA - bB$. The final values chosen for the four parameters $v_{N\infty}$, $v_N(0)$, γ and δ are shown in Fig. 8.

2. *Prediction of $g_{Na}(t)$ under a Voltage Clamp*

The above results, obtained by fitting the mathematical model to the specific clamps given in fig. 6 of HH (2), can be used to predict the behavior of $g_{Na}(t)$ during any arbitrary clamp. For example, taking the case of a clamp to $V = 70$ mv, the smooth curves of Fig. 8 give the values: $v_{N\infty} = 17.3$, $\dot{v}_N(0) = 280$/msec, $\gamma = 5.40$/msec, $\delta = 3.80$/(msec)^2. These in turn lead to the values: $A = 71.0$, $B = 53.7$, $a = 4.57$/msec, $b = 0.83$ msec., so that v_N becomes

$$v_N = 71.0(1 - e^{-4.57t}) - 53.7(1 - e^{-0.83t}).$$

Using the $v_N(t)$ computed from the above equation, the corresponding $g_{Na}(t)$ values are read off of the curve of Fig. 7. The resulting $g_{Na}(t)$ curve is shown in Fig. 22.

APPENDIX III—*Physical Model for g_K*

Let us assume that the (passive) transport of potassium ions takes place at specific *regions* along the membrane. Further let us assume that each of these regions can exist in any one of $p + 1$ states, but that K activation occurs for only one of these $p + 1$ states. Two distinct types of situations, requiring different statistical treatment, can be distinguished and one example of each is discussed below.

As an example of the first type consider the situation suggested by HH (2). In this case the regions could be specific locations along one of the membrane surfaces, each region containing p sites for the binding of specific activating molecules. The $p + 1$ states of a region would then consist of occupancy on the binding sites of $0,1,2,\ldots.p$ activating molecules. All p sites of a given region must be occupied in order for K^+ ions to be able to pass through the membrane at that region. Thus, only one out of the $p + 1$ possible states gives rise to potassium conductance.

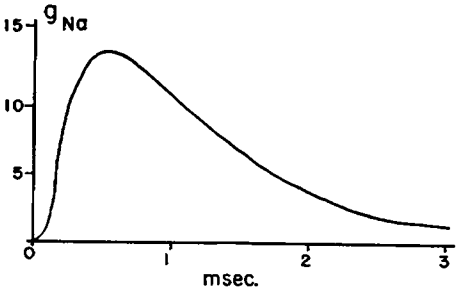

FIGURE 22 Predicted variation of $g_{Na}(t)$ for a clamp of 70 mv, obtained using the curves of Figs. 7 and 8. The ordinate scale is in mmho/cm^2.

As an example of the second type, imagine that each of the regions consists of a pore through the membrane with each pore containing p polar side chains that can project into it. Suppose further that each polar side chain has two possible orientations, one that blocks the passage of K^+ ions and one that allows their passage, and that an energy barrier separates them. The $p + 1$ states for each pore (region) then consist of $0,1,2,\ldots,p$ of these side chain gates being in the open rather than the closed position. All p gates of a given pore must be in the open position in order for K^+ passage through the pore to be possible. Again only one out of the $p + 1$ possible states gives rise to potassium conductance.

The initial stages of the analysis of both types are the same. The discussion will be given in terms of the pore plus gates model. However translation to the regions plus binding sites model can be made by substitution of the words region for pore, binding site for gate, occupied site for open gate, and unoccupied site for closed gate.

The energy difference between the closed and open positions of any one gate will be denoted by ϵ. This energy difference will be dependent on the electric potential difference across the membrane, and will be assumed to be the same for each gate. Since the closing of any one gate in a pore is assumed to effectively prevent the passage of K^+ ions through that pore, the potassium conductance of the membrane will be determined by the fraction of pores that have all p gates open, P_p. Thus if g_0 is the conductance of a pore with all gates open, and if there are N pores per unit area of membrane, the conductance per unit area will be given by $g = g_0 N P_p$.

According to Boltzmann statistics, in equilibrium the fraction of gates open, irrespective of the pore in which they lie, will be given by

$$y = \frac{e^{-\epsilon/kT}}{1 + e^{-\epsilon/kT}}. \tag{A1}$$

Thus y represents the probability that any one gate is open, and $(1 - y)$ the probability that it is closed. For the HH model, y would represent the probability that any one binding site is occupied by one of the activating molecular species, and $(1 - y)$ the probability that the binding site is not occupied. In this case ϵ represents, for one of the (ionic) molecular species, the energy difference between a position on the "wrong" and on the "right" side of the membrane.

In the case of independent molecular events the probability, P_p that any one region has all of its p sites occupied is given quite simply by

$$P_p = y^p \tag{A2}$$

leading to $g = g_0 N y^p = \bar{g} y^p$, the HH (2) and Cole and Moore (1) case.

For the case of a collection of dipoles with two stable orientations, the situation may not be as simple. The p dipoles within one pore may form a resonant system in which a single activation unit of energy, ϵ, representing one dipole gate in the open position, must be considered as shared between all p gates of the pore rather than as concentrated in one particular dipole. Such a situation is analogous to the delocalized "exciton" discussed by Kasha (13). In such a situation each pore, with its p gates, must be considered as a single system. The number of energy units possessed by the pore (number of open gates) can be specified, but this energy cannot be assigned among the specific gates of the pore. The situation is thus different from the case of the binding of large molecular ions to specific sites of a given region. In the latter case it is possible not only to specify how many of the binding sites of a given region are occupied, it is also logically possible for example to specify that it is site a that is occupied and site b that is unoccupied, logically possible to the extent that under the given physical conditions the occupying molecular ions can be described by classical physics. While quantum effects are large for the electrons that form the covalent bonds in molecules, molecules themselves behave very much as classical particles. Photons of energy on the other hand must of necessity be treated quantum mechanically. In particular, Eq. (A2) is not valid for the quantum case of p dipoles that form a single resonant system. A derivation of the equation that applies for this latter quantum case is given below.

Since the opening of any one gate requires an energy ϵ, a pore with j gates open can be considered as a system possessing an amount of energy given by $j\epsilon$. A pore can thus be considered as a quantum system with a ground state (all gates closed) and p excited states (1,2,. . . .p gates open). A collection of such pores will then obey Boltzmann statistics, the fraction in the pth excited state being given by

$$P_p = \frac{e^{-p\epsilon/kT}}{\sum_{j=0}^{p} e^{-j\epsilon/kT}}$$

Performing the geometric sum in the denominator, one obtains

$$P_p = \frac{e^{-p\epsilon/kT}(1 - e^{-\epsilon/kT})}{1 - e^{-(p+1)\epsilon/kT}}. \tag{A3}$$

The substitution of $y = \frac{e^{-\epsilon/kT}}{1 + e^{-\epsilon/kT}}$ from Eq. (A1) then leads to

$$P_p = \frac{1 - 2y}{y\{[(1 - y)/y]^{p+1} - 1\}}. \tag{A4}$$

Eq. (A4) for $P_p(y)$ is plotted in Fig. 23 for several values of p, together with the curve for $g_E(v_k)$ determined earlier (Fig. 2). It is seen that the points for $p = 9$ differ so little from the experimental curve that over most of the range the two cannot be distinguished. The divergence of the $p = 8$ and $p = 10$ cases is more apparent in this figure than is strictly the case. The scale chosen for P_9 is that which brings the P_9 points into the best agreement with the experimental curve. Different choices of scale can bring the P_8 and P_{10} points into better agreement, though not as close as that shown for the P_9 case.

With a sudden change in membrane voltage such as occurs in a voltage clamp there is an accompanying sudden change in ϵ, the energy difference between an open and a closed gate. The physical picture implied by the above model can then be described as

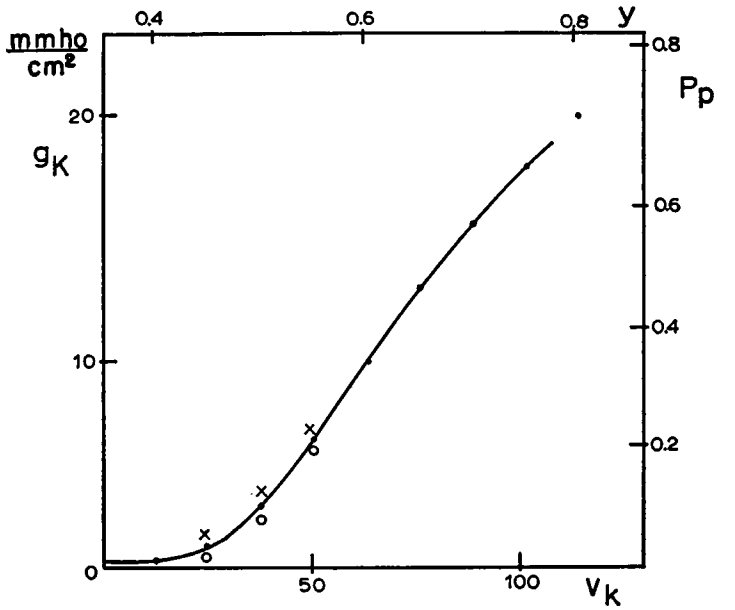

FIGURE 23 Variation of g_K with v_k, and of $P_p = 1 - 2y/y\{[(1 - y)/y]p^{*1} - 1\}$ with y. The smooth curve is a reproduction of the empirically determined curve for $g_K(v_k)$ of Fig. 2. The calculated values of P_p are shown by points for $p = 9$; where the calculated values for $p = 10$ and $p = 8$ differ from those for $p = 9$, they are shown by crosses and circles, respectively.

follows. Suppose that the relaxation time constant, τ_p, for the system of gates to come into thermodynamic equilibrium and be describable by a temperature, T_p, is very short compared to the relaxation time constant, τ_k, for the system of gates to come into temperature equilibrium with the surroundings. The picture is then somewhat analogous to the spin-magnetic dipole problem of solid state physics when the spin-spin relaxation time constant is very short compared to the spin-lattice time constant. Before the clamp is applied the difference between the closed and open positions is ϵ_0, the gate system and surroundings are in temperature equilibrium at a temperature T_0, and the fraction of open gates is given by

$$y_0 = e^{-\epsilon_0/kT_0}/(1 + e^{-\epsilon_0/kT_0}). \tag{A5}$$

Immediately after the voltage clamp is applied the fraction of open gates is still y_0, but the energy difference between the open and closed positions is now ϵ_1, and the temperature of the system of gates is correspondingly changed to T_1 given by

$$y_0 = e^{-\epsilon_1/kT_1}/(1 + e^{-\epsilon_1/kT_1}). \tag{A6}$$

With the passage of time the temperature of the gate system will gradually return from T_1 to T_0, and the fraction of open gates will correspondingly change (with a time constant τ_k) from y_0 to y_1 where y_1 is given by

$$y_1 = e^{-\epsilon_1/kT_0}/(1 + e^{-\epsilon_1/kT_0}). \tag{A7}$$

The fraction of pores with all p gates open will correspondingly change from $P_p(y_0)$ to $P_p(y_1)$ where P_p is given by Eq. (A4).

The fact that the curve of Fig. 23 cannot be fitted by a power law but can be fitted by Eq. (A4) supports the choice of the unit model composed of 9 coordinated dipoles sharing a set of quanta of energy (excitons) in accordance with (A3). Thus, each collection of 9 dipoles shares a number of units of energy ϵ in such a way that each dipole remains energetically independent, having just two levels separated by an energy ϵ. (This last condition justifies the substitution of (A1) into (A3).) Although the model has been discussed in terms of reorienting polar side chains, other specific models of the same class are also possible; for example, the displacements of protons in hydrogen bonds from one to another stable position.

Kinetic Analysis

The variation of g_K with v_k has been shown to be satisfactorily accounted for by a model that involves gates with two orientations, differing in energy. Thus g_K is given by $g_K = g_0 N P_9(y)$ where $P_9(y)$ is given by Eq. (A4) with $p = 9$, N is the number of pores or potassium regions along the membrane and g_0 is the conductance of a pore with all gates open. The linear transformation between y and v_k that brings the $g_K(v_k)$ curve into coincidence with $P_9(y)$ is $y = 0.357 + 0.00394\, v_k$.

In addition to the variation of g_K with v_k, two other requirements of any complete theory are that it account for the dependence on membrane voltage, shown in Fig. 3, of both the rate constant, $a_k = 1/\tau_k$, and the maximum equilibrium value of v, $v_{k\infty}$. The latter is given by Eq. (A1), but will be derived again in the kinetics analysis given below. This analysis is given in terms of the polar side chain gate model, but can be equally applied to the hydrogen bond and other similar models.

Assume that each side chain has two stable positions represented by the potential wells of Fig. 24. Case (a) represents the situation at the resting voltage and case (b) that at some depolarizing voltage V. The time-dependent equation for the variation of the relative number of dipoles in the right-hand well (open gate) is

$$\frac{dy}{dt} = -(k_1 + k_2)y + k_1, \tag{A8}$$

where k_1 and k_2 are the rate constants for jumps in the two directions as indicated in the figure. The over-all rate constant is therefore given by

$$a_k = \frac{1}{\tau_k} = k_1 + k_2, \tag{A9}$$

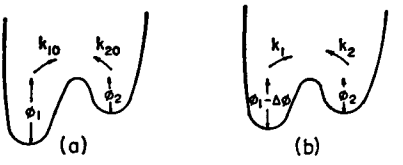

FIGURE 24 Double potential well model. In the resting state the energy barrier heights are ϕ_1 and ϕ_2 as shown in case (a). The rate constants for transitions from left to right and right to left, k_1 and k_2, respectively, depend on the barrier heights. When the membrane voltage is changed, as in case (b), the barrier heights change and the rate constants correspondingly change.

and the equilibrium value of y is given by

$$y_\infty = \frac{k_1}{k_1 + k_2}. \tag{A10}$$

If $\Delta\phi$ is the effective potential energy change at the dipole site, assumed to be linearly related to the displacement, V, of the membrane potential, then k_1 and k_2 will be given by

$$k_1 = Ke^{-(\phi_1 - \Delta\phi)/kT}, \tag{A11}$$

$$k_2 = Ke^{-\phi_2/kT}. \tag{A12}$$

For simplicity only the left-hand barrier height is assumed to change with V. The magnitude of K can not be predicted theoretically without a detailed knowledge, presently lacking, of the structure of the surrounding membrane. Using Eqs. (A11) and (A12), Eqs. (A9) and (A10) become, respectively,

$$a_k = Ke^{-\phi_1/kT}e^{\Delta\phi/kT} + Ke^{-\phi_2/kT} = ae^{\Delta\phi/kT} + b, \tag{A13}$$

$$y_\infty = \frac{e^{-(\phi_1 - \phi_2 - \Delta\phi)/kT}}{1 + e^{-(\phi_1 - \phi_2 - \Delta\phi)/kT}} = \frac{e^{-\epsilon/kT}}{1 + e^{-\epsilon/kT}}, \tag{A14}$$

where $\epsilon = \phi_1 - \phi_2 - \Delta\phi$ is the energy difference between the two wells. The latter equation is in agreement with Eq. (A1).

The exponential dependence of a_k on the membrane voltage, predicted by Eq. (A13), is shown in Fig. 25(a) to be in approximate agreement with the experimental points. The

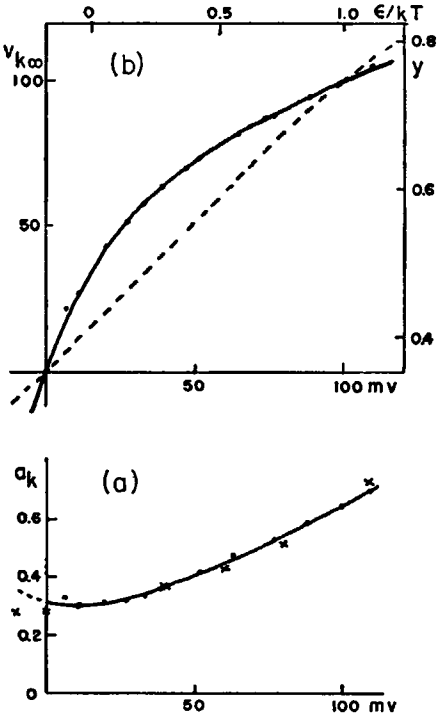

FIGURE 25 (*a*) Dependence of a_k on the membrane voltage. The points and the solid curve are a reproduction of the points and curve of Fig. 3*b*, chosen to fit the clamp data. The crosses are computed according to the equation $a_k = 0.220 + 0.070 \exp 0.0182\ V$, where V is in millivolts. The ordinate scale is in $(\text{msec.})^{-1}$. (*b*) Dependence of $v_{k\infty}$ on V. The points, ·, and the solid curve are reproductions of Fig. 3*a* and were chosen to give the best fit to the clamp data. The dashed curve represents an attempt to fit the data to Eq. (14).

divergence from the dashed extrapolated curve used for the calculation of membrane action potentials is not to be considered as serious. The form of the action curves is but little changed if a_k is assumed to follow the prediction of Eq. (A13). Alternatively, if in Fig. 24 the barrier height for crossing from right to left is assumed to change as well as the barrier height for crossing from left to right, the expression for a_k of Eq. (A13) will become

$$a_k = ae^{\Delta\phi_1/kT} + be^{-\Delta\phi_2/kT}$$

where the net change in level of the wells is given by $\Delta\phi = \Delta\phi_1 + \Delta\phi_2$. Such an expression for a_k would allow the possibility of a second rising region for negative values of V. However, what may be a serious difficulty arises when the relative magnitudes of $\Delta\phi$ are compared. It is found from the analysis of Fig. 25*a* that for a 100 mv change in membrane voltage the change $\Delta\phi$ is 45 electron millivolts. Such a large value for $\Delta\phi$ would not allow the series arrangement of 9 dipoles of reasonable dipole moment in each pore that the present theory seems to require.

The same difficulty arises when the behavior of the equilibrium value of y is compared with that of $v_{k\infty}$. A comparison of the abscissa for the $g_K(v_k)$ and the $P_s(y)$ curves of Fig. 23 shows that as v_k varies from 0 to 100, y varies from 0.354 to 0.747, and Eq. (A1) implies in turn that ϵ should vary from $+0.015$ to -0.027 electron volts. This means that for a 100 mv change of membrane voltage the energy difference between an open and closed gate must change by about 42 electron mv, in good agreement with the 45 electron mv found from the a_k data, and like it a value that seems unreasonably high. A further difficulty lies in the fact that according to the above picture the curve for $v_{k\infty}$ *versus* V should be fitted by Eq. (A14) which it obviously is not, as Fig. 25(*b*) clearly shows. Many of the same difficulties appear if the analysis of HH is pushed to similar limits. A possible way of overcoming these difficulties in the present case may lie in the model of distortionable double wells discussed by Fuchs and von Hippel (14). As shown by Fuchs and von Hippel, such a model can lead to both polarization curves that differ from the normal one of Eq. (A1) and to much reduced polarizing fields for the same degree of polarization.

In spite of the above mentioned difficulties this model has been successfully used to compute the delays that would result from large and long lasting hyperpolarizing preclamps. It is shown in the Discussion that the predicted delays are sufficient to account for the results of Cole and Moore (1).

This work was supported in part by a Research Grant from the National Science Foundation.

Received for publication, July 13, 1962.

REFERENCES

1. COLE, K. S., and MOORE, J. W., *Biophysic. J.*, 1960, **1**, 1.
2. HODGKIN, A. L., and HUXLEY, A. F., *J. Physiol.*, 1952, **117**, 500.
3. TASAKI, I., and HAGIWARA, S., *J. Gen. Physiol.*, 1957, **40**, 859.
4. TASAKI, I., and SPYROPOULOS, C. S., *Am. J. Physiol.*, 1958, **193**, 318.
5. FITZHUGH, R., *J. Gen. Physiol.*, 1960, **43**, 867.
6. NOBLE, D., *J. Physiol.*, 1962, **160**, 317.
7. COLE, K. S., and MOORE, J. W., *J. Gen. Physiol.*, 1960, **44**, 123.
8. HODGKIN, A. L., HUXLEY, A. F., and KATZ, B., *J. Physiol.*, 1952, **116**, 424.
9. HODGKIN, A. L., and HUXLEY, A. F., *J. Physiol.*, 1952, **116**, 449.

10. HODGKIN, A. L., and HUXLEY, A. F., *J. Physiol.*, 1952, **116**, 473.
11. HODGKIN, A. L., and HUXLEY, A. F., *J. Physiol.*, 1952, **116**, 497.
12. MULLINS, L. J., *J. Gen. Physiol.*, 1958, **42**, 1013.
13. KASHA, M., *in* Biophysical Science—A Study Program (J. L. Oncley, editor), 162.
14. FUCHS, R., and VON HIPPEL, A., *J. Chem. Physics*, 1961, **34**, 2165.
15. NACHMANSON, D., and WILSON, I. B., *in* Electrochemistry in Biology and Medicine, (T. Shedlovsky, editor), New York, John Wiley & Sons, Inc., 1955, 167.